Quantum Chemical Investigation of Thermotropic Ionic Liquid Crystals to Predict Phase Transition Temperatures

Erin Makara
VTT, Vuorimiehentie 2, 02150 Espoo, (*Finland*)

***Abstract*— The need for higher capacity and efficient energy storage solutions for renewable energy sources and electric vehicles has resulted in renewed focus on the development of high-capacity lithium metal batteries (LMBs). Dendrite growth caused by uneven lithium ion electrodeposition is the most significant obstacle to the safe and successful use of LMBs, as it can lead to battery malfunction and fire hazards. Thermotropic ionic liquid crystals (TILCs) are a combination of liquid crystal and ionic compounds which provide both dendrite inhibition and self-healing electrolyte (SHE) properties. In this short version of the thesis, the results from DFT calculations of 10 TILCs and 11 non-ionic thermotropic liquid crystals are explored. A strong correlation between experimental liquid–liquid crystal phase transitions and various quantities obtained through DFT was found and transition temperatures were predicted for additional molecules. Additionally, recommendations were made for TILCs with lower transition temperatures than those of the source material. Furthermore, the use of multivariate regression and machine learning (ML) was suggested for a more reliable model, and an automated computational workflow model for high-throughput DFT calculations using TURBOMOLE was presented.**

***Index Terms*—Dendrites, density functional theory, lithium metal batteries, thermotropic ionic liquid crystals, self-healing electrolyte**.

I. Introduction

Energy storage has become increasingly critical in recent times. The emergence of renewable sources of energy, such as wind and solar, has the capability to eventually replace fossil fuels, but without a suitable energy storage system they remain problematic. This is especially relevant now as political issues and a global conflict have caused fossil fuel prices to spike in Europe.[1]

Storage is necessary to balance out the electric output when renewable sources are connected to the grid, particularly with an electric input of over 10%.[2]

Additionally, the transportation sector is working towards electrifying vehicles in order to reduce fossil fuel and CO_2 emissions. Norway is aiming to have all of its cars either electric or hybrid by 2025. Batteries are the primary concern as they have the most drawbacks such as high prices, limited range, long charging times, short lifespans and safety issues.[2, 3]

The biggest issue with high-performance lithium batteries is dendrite growth on the anode, which eventually causes a short-circuit. To tackle this, various methods have been proposed, such as alloying structure, organic electrolyte- and solid-liquid interface design, solid electrolyte, and novel architecture design.[4]

Liquid crystal an intermediate state form of a substance between a liquid and a solid crystal, but possesses the properties of both. A thermotropic liquid crystal attains different phase states at different temperatures, i.e. the temperature affects the order parameter.[5, 6] Ionic liquid crystals comprise of cations and anions (usually consisting of a charged large molecule and a single ion coupled to it) which provides conductivity. A thermotropic ionic liquid crystal (TILC) combines both into a versatile material capable of dynamic molecular order and self-assembling ability, with anisotropic physical properties, ionic conductivity, fine-tuning possibilities, salt addition, and more.[7–9]

TILCs can be used in countering dendrite growth as a self-healing electrolyte (SHE), where in its liquid crystal state it acts as any battery electrolyte, but when heated up to change into an isotropic state, it snaps off the formed dendrites. This is a particular focus of HIDDEN, a EU Horizon 2020 project aiming to create feasible lithium self-healing batteries (SHBs).[10]

New tools and workflows were created in the thesis in order to compute various TILC electrolytes in bulk, and a correlation to predict their phase transitions from isotropic liquid to smectic was found using data produced by Mizumura *et al.*[11]. Insight was gained on how to modify the molecular architecture to find an electrolyte with the right temperature specifications for use in self-healing batteries. Supplementary data by Mandle *et al.*[12] was also used. This short version of the thesis presents only the computational part of the original thesis.[13]

II. Research Material and Methods

The purpose of this project was to create tools and a workflow for DFT calculations on different TILC electrolytes, and to automate the process to make bulk calculations possible. Additionally, the aim was to discover any correlations between experimental TILC phase transition values and computational output, and to generate data for potential post-processing with machine learning. This research was conducted to find suitable TILCs to be used as electrolytes in lithium batteries, as those with transition temperatures from and to the isotropic phase higher than 60°C are more common than those lower.[14] The goal was to find TILCs with a transition temperature below 60°C.

A. *Computational Details*

All calculations were performed in TURBOMOLE[15, 16] using Density Functional Theory (DFT)[17, 18] with the PBE0[19, 20] exchange-correlation functional, Resolution of Identity approximation for Coulomb integrals (RI-J),[21–23] Multipole Accelerated RI-J (MARIJ)[24], and def2-TZVP[25, 26] basis set. Computations were done on CSC servers.

Geometrical structures of the investigated molecules were computed in gas phase. The structures were optimized until the resulting energies converged to the lowest energy. Vibrational frequencies and thermodynamic properties were thus calculated using the optimized structure. All molecules have been confirmed to be stable by making sure there were no imaginary frequencies.

B. *Molecules*

The blocks used to build the molecules are shown in Tables I, II, and III. The promesogenic group attaches to the left of the linker group, and the functional group attaches to the right of the linker group. Some groups have been omitted as no molecule in this thesis uses them.

TILCs with existing experimental data for their phase transition temperatures were sourced from Mizumura *et al.*[11] and Mandle *et al.*[12] and are shown in Tables IV and V respectively. Additional molecules that have been simulated are shown in Table VI.

A particular note on the molecules of Mizumura *et al.*—the original paper makes no comment on whether stereoisomers were taken into account. In particular, the functional group g0 (and its derivative g0c) has chirality[27] and the aliphatic ring in the promesogenic group m1 also has more than one conformers.[28] Stereoisomers have not been taken into account in this thesis, however, the workflow (designed for high throughput) presented allows them to be included without problem in future calculations and analysis.

TABLE I
Promesogenic groups

Label	Molecule
m1.n	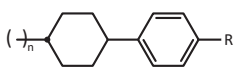
m2	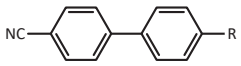
m3	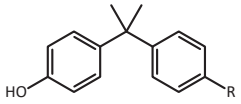
m4	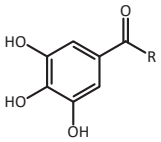

TABLE II
Linker groups

Label	Molecule
b1.n	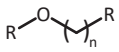
b1b.n	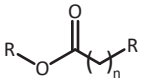
b2.n	
b3.n	

TABLE III
Functional groups

Label	Molecule
g0	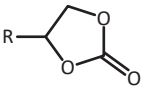
g0c	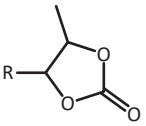
g4.n	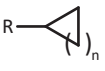

TABLE IV
SOURCE MOLECULES BY MIZUMURA *et al.*[11]

Label	Molecule Parts
KATO1 A/ m1.5-b1.3-g0	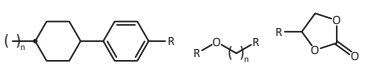
KATO1 A/ m1.5-b1.4-g0	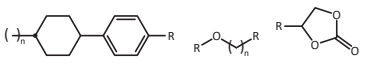
KATO1 A/ m1.5-b1.5-g0	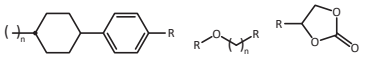
KATO1 A/ m1.5-b1.6-g0	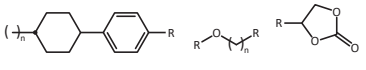
KATO1 A/ m1.5-b1.7-g0	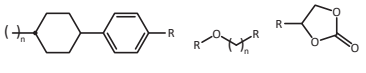
KATO1 A/ m1.5-b1.8-g0	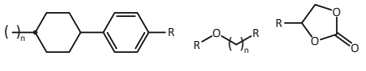
KATO1 A/ m1.5-b1.9-g0	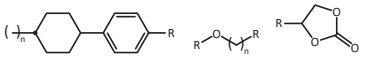
KATO1 B/ m1.5-b3.2-g0	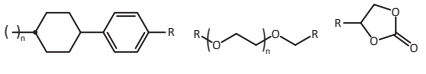
KATO1 B/ m1.5-b3.3-g0	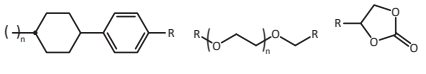
KATO1 B/ m1.5-b3.4-g0	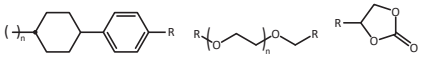

TABLE V
SOURCE MOLECULES BY MANDLE *et al.*[12]

Label	Molecule Parts
GOOD1 A/ m2-b1.3-g4.1	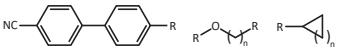
GOOD1 A/ m2-b1.3-g4.2	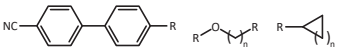
GOOD1 A/ m2-b1.3-g4.3	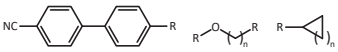
GOOD1 A&B/ m2-b1.3-g4.4	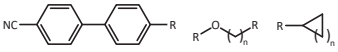
GOOD1 A/ m2-b1.3-g4.5	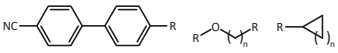
GOOD1 B/ m2-b1.1-g4.4	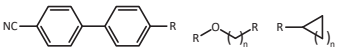
GOOD1 B/ m2-b1.2-g4.4	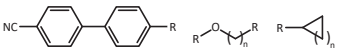
GOOD1 B/ m2-b1.4-g4.4	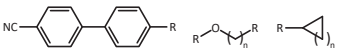
GOOD1 B/ m2-b1.5-g4.4	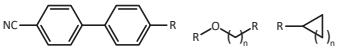
GOOD1 B/ m2-b1.6-g4.4	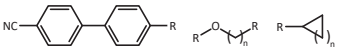
GOOD1 C/ m2-b1b.4-g4.4	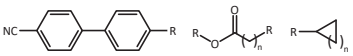

TABLE VI
ADDITIONAL MOLECULES SIMULATED

Label	Molecule Parts
MESO1 A/ m1.3-b1.[2-6]-g0	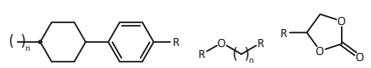
MESO1 B/ m1.4-b1.[2-6]-g0	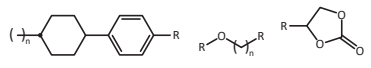
MESO2 A/ m2-b1.[2-6]-g0	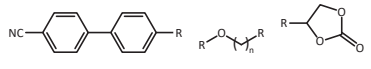
MESO2 B/ m3-b1.[2-6]-g0	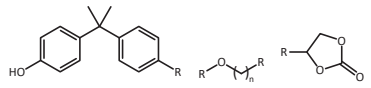
MESO2 C/ m4-b1.[2-6]-g0	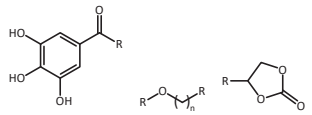
REV1/ m1.[5-8]-b3.4-g0c	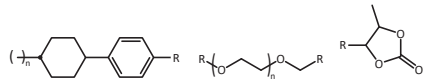

III. RESULTS

The calculations provided energy information, electrostatic moments, thermochemical information, IR-, Raman- and excitation spectra, NMR shielding constants and more, though a smaller subset of them was used.

The zero point vibrational energy (ZPE) and experimental phase transition temperatures for the reference molecules are presented in Tables VII and VIII.

A. *Analysis*

Phase transition temperatures were plotted against total electronic energy, HOMO-LUMO gap energy, zero point vibrational energy, molar mass, molecule length, absolute dipole moment, and the thermochemical intersection points, shown in Figures 1, 2, and3. Various patterns emerged in these graphs.

The overall correlation between the KATO1 set in the total electronic energy, ZPE, molar mass, and the thermochemical intersection point graphs is quite clear. The correlation with ZPE is particularly great, with both subsets closely aligned. Conversely, the graphs of molecule length and absolute dipole moment are quite erratic. Although the length graph is chaotic in this set, it could be used for different transition temperatures, such as the smectic–crystal phase transition. Mizumura *et al.* did mention that the length changes with each extra carbon in the linker, following a pattern similar to the other transition temperature. Hence, length could be used in the future to look for correlations.

TABLE VII
RESULTS OF THE MIZUMURA *et al.* SET. ZERO POINT VIBRATIONAL ENERGY AND PHASE TRANSITION TEMPERATURES FROM ISOTROPIC TO SMECTIC.[11]

Molecule	ZPE (kJ mol^{-1})	T_{Sm}^{ISO} (°C)
KATO1 A		
m1.5-b1.3-g0	1417	102
m1.5-b1.4-g0	1493	96
m1.5-b1.5-g0	1567	89
m1.5-b1.6-g0	1643	76
m1.5-b1.7-g0	1717	72
m1.5-b1.8-g0	1792	61
m1.5-b1.9-g0	1868	60
KATO1 B		
m1.5-b3.2-g0	1593	91
m1.5-b3.3-g0	1754	70
m1.5-b3.4-g0	1917	54

TABLE VIII
RESULTS OF THE MANDLE *et al.* SET. ZERO POINT VIBRATIONAL ENERGY AND PHASE TRANSITION TEMPERATURES FROM NEMATIC TO ISOTROPIC.[12]

Molecule	ZPE (kJ mol^{-1})	T_{ISO}^{N} (°C)
GOOD1 A		
m2-b1.3-g4.1	875.8	48
m2-b1.3-g4.2	952.3	62
m2-b1.3-g4.3	1031	75
m2-b1.3-g4.4	1108	84
m2-b1.3-g4.5	1184	74
GOOD1 B		
m2-b1.1-g4.4	959.8	—
m2-b1.2-g4.4	1033	—
m2-b1.3-g4.4	1108	84
m2-b1.4-g4.4	1184	55
m2-b1.5-g4.4	1258	85
m2-b1.6-g4.4	1332	—
GOOD1 C		
m2-b1.5-g4.4	1258	85
m2-b1b.4-g4.4	1207	76

For the GOOD1 set, the correlations are not as strong, but there are still some discernible patterns in the total electronic energy and thermochemical intersection point graphs. Conversely, the molecule length and absolute dipole moment graphs show a better correlation, particularly in comparison to the chaotic nature of the KATO1 set. Notably, both of these graphs accurately depict the trend of increasing the number of carbons in the g4 functional group (aliphatic ring).

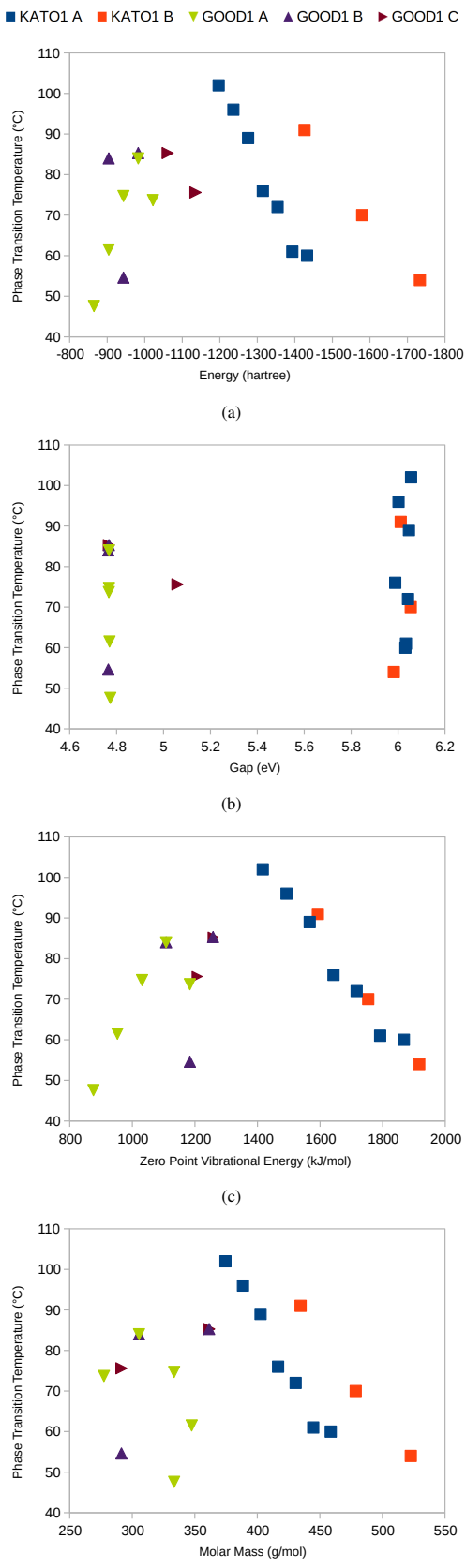

Fig 1. Phase transition temperatures (T_{Sm}^{ISO} for KATO1 and T_{ISO}^{N} for GOOD1) plotted against the electronic energy (a), HOMO-LUMO gap energy (b), zero point vibrational energy (c), and molar mass (d).

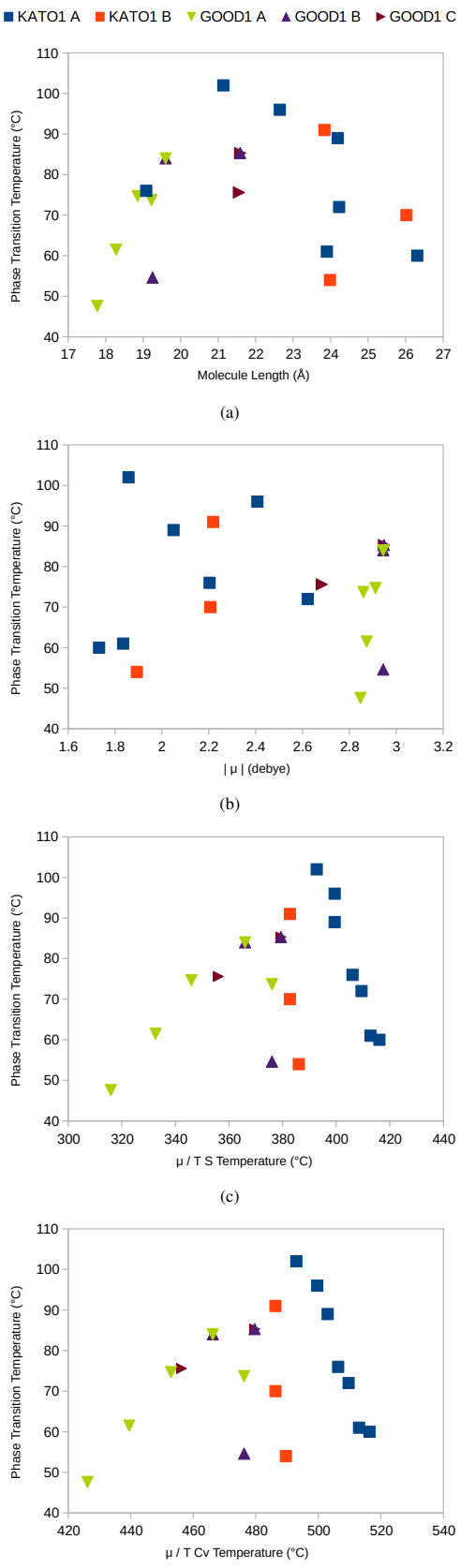

Fig 2. Phase transition temperatures (T_{Sm}^{ISO} for KATO1 and T_{ISO}^{N} for GOOD1) plotted against the molecule length (a), absolute dipole moment (b), chemical potential and entropy intersection point (c), and isochoric heat capacity intersection point (d).

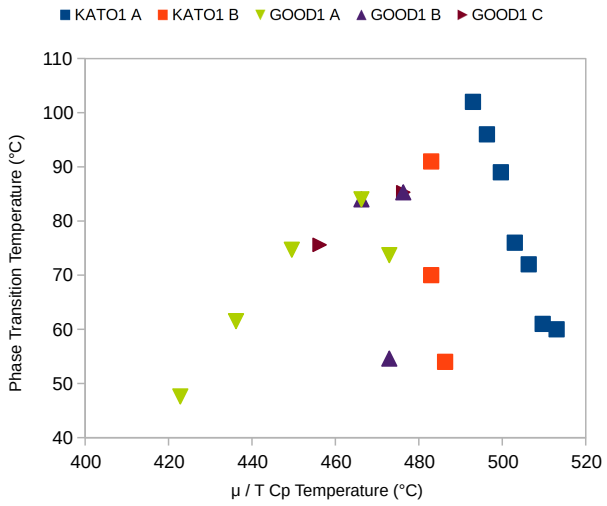

Fig 3. Phase transition temperatures (T_{Sm}^{ISO} for KATO1 and T_{ISO}^{N} for GOOD1) plotted against the isobaric heat capacity intersection point.

It is worth pointing out that the lengths obtained were calculated using a convex hull algorithm, which merely finds the two most distant atoms and calculates the distance between them. However, the value determined as a result may not accurately reflect the true length if the molecule is not entirely linear, i.e. if it is bent or twisted. These results are applicable to single molecules only; hence, more accurate results require multiple calculations, particularly if there are multiple conformers. It is usually recommended to take the average of the results obtained, but it is rational to consider the maximum value in this case since the molecule should be in its most linear form. The lengths obtained however agreed with those obtained by Mizumura *et al.* and Mandle *et al.*

The HOMO-LUMO gap energy graph of the KATO1 and GOOD1 sets showed that the molecules of both sets settled around their own values ($\approx$ 6.0 eV for KATO1, $\approx$ 4.8 for GOOD1), with the exception of the GOOD1 C molecule with the b1b linker (ester group). This might be used as a way to check the similarity and applicability of a model.

Unfortunately, the KATO1 and GOOD1 sets are not compatible due to two factors: firstly, the intention of the thesis is to investigate TILCs, of which the KATO1 molecules are a part. The GOOD1 molecules, however, are not ionic. Secondly, the reported transition temperatures are related to different transitions. The liquid crystal phase prior to the complete liquid phase is different for each set (smectic for KATO1, nematic for GOOD1), in addition to the direction of the temperatures (reported on cooling for KATO1, and on heating for GOOD1). Therefore, the thesis mainly focused on the KATO1 data set for the purpose of creating a predictive model.

Going back to the KATO1 set, it was observed that out of all the graphs, ZPE had the best correlation with itself, an unexpected yet fortunate occurrence. While this correlation may be useful for molecules similar to those in the KATO1 set, there is no proof that it can be applied to TILCs that differ too much. Nevertheless, predictions for these different molecules can be investigated.

It is reasonable to assess ZPE's usefulness for correlation purposes. ZPE is a measure of the kinetic energy of a system at its lowest point, and is non-zero unlike in classical physics. Generally, the value of ZPE increases with the size and rigidity of a molecule. A higher ZPE implies that the molecule has more capacity to absorb kinetic energy. For example, adding more alkyl-chains increases the molecule's ability to rotate, bend and stretch, thereby increasing ZPE. On the other hand, adding rigid bonds or converting an aliphatic ring into an aromatic one reduces ZPE. In summary, ZPE can be a helpful indicator of molecule flexibility which in turn influences liquid crystal behavior.[29, 30]

Considering the above, a linear trend line could be plotted for the ZPE graph, with its equation and graph shown in Figure 4. The coefficient of determination (R^2) was 0.9676. Using this correlation function, the trend line's equation can be used to calculate and predict ISO-Sm phase transition temperatures for other similar molecules. Furthermore, there is potential to make use of the quantities with subset correlations to generate data for post-processing using data-driven techniques, such as machine learning, which may result in a better way of predicting TILC phase transitions.[31, 32]

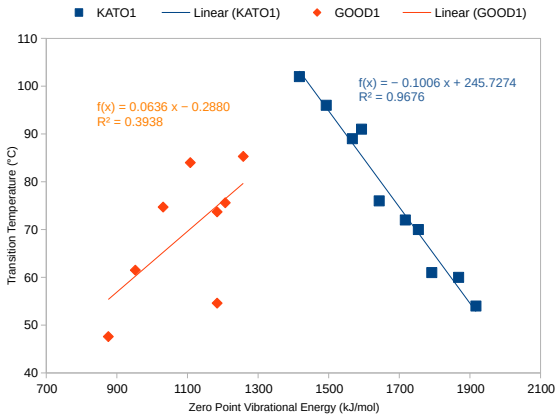

Fig 4. Phase transition temperatures (T_{Sm}^{ISO} for Mizumura *et al.* and T_{ISO}^{N} for Mandle *et al.*) plotted against zero point vibrational energy.

The model obtained suggests that higher ZPE correlates with lower ISO-Sm phase transition temperature, which is logical when taking into account that greater structural rigidity can be beneficial for mesomorphic behavior, and which structures lead to higher ZPE. It should be taken into consideration though, that despite being inconsistent, the GOOD1 set with a similar trend line construction, predicts the exact opposite. Until more data points of various TILCs are acquired for the model, it is wise to remain skeptical when applying the model to TILCs with significantly different promesogenic and functional groups.

B. *Predictions*

Table IX contains the total electronic energies, HOMO-LUMO gap energies, zero point vibrational energies, molar masses, molecule lengths, absolute dipole moments, thermochemical intersection points and predicted ISO-Sm phase transition temperatures, with a margin of error of $\pm 12°C$.

The MESO1 set mainly varied from the KATO1 set in the length of the alkyl-chain in the mesogenic group, which reflects on their ZPE values and is in line with the prior reasoning of the quantity.

The MESO2 set explored three mesogenic groups: a cyanobiphenyl (m2), a bisfenol (m3) and a gallic acid (m4). The model indicates that the bisfenol mesogenic core has the lowest transition temperatures of the three, followed by the cyanopiphenyl and the gallic acid, all higher than the KATO1 set. The REV1 set was derived from the KATO1 B molecules based on the findings of the MESO sets and understanding of ZPE, where the functional group was changed from an ethylene carbonate (EC) to a propylene carbonate (PC) group and the length of the alkyl chain in the promesogenic group was increased.

The model predicts the REV1 molecules have a lower transition temperature than the KATO1 B subset. For example, the m1.5-b3.4-g0 and m1.5-b3.4-g0c molecules show that the addition of the methyl group to the functional group reduces the transition temperature from 54°C to 46°C ($\pm 12°C$). Further lengthening the tail of the mesogenic group reduces it to 38°C, 31°C, and finally to 23°C ($\pm 12°C$). The data from Mizumura *et al.* does not show crystal-smectic phase transitions above 0°C for the KATO1 B subset, which suggests the same for the REV1 molecules. However, the efficacy of changing the ethylene carbonate to a propylene carbonate group is still uncertain due to the "EC-PC mystery" which involves differences in reactivity and degradation products. Nevertheless, it should not be a problem since PC has mainly been problematic with graphite due to the co-intercalation with Li^+ ions, which should not be a problem with a much larger molecule.[33]

Despite the successful correlation found, caution should be taken when considering the applicability of the constructed model. To further the model's predictive power, more data and variables might be taken into account through multivariate regression and ML techniques. Additionally, the liquid crystal phase phenomena are related to inter-molecular interaction and bonding, which single-molecule calculations ignore. Multi-molecular systems can be simulated through DFT, though this is computationally expensive and has its own issues. However, data-driven techniques such as ML-DFT could be used to make multi-molecular calculations more feasible, which could then be used to improve the predictive models of macro-scale properties, like transition temperatures. The HIDDEN project's experimental researchers can use these predictions as a starting point to potentially confirm or refute them.[10]

TABLE IX
RESULTS OF THE ADDITIONAL MOLECULE SETS. ZERO POINT VIBRATIONAL ENERGY AND THE PREDICTED PHASE TRANSITION TEMPERATURES FROM ISOTROPIC TO SMECTIC.

Molecule	ZPE (kJ mol^{-1})	T_{Sm}^{ISO} (°C)
MESO1 A		
m1.3-b1.2-g0	1197	125
m1.3-b1.3-g0	1271	118
m1.3-b1.4-g0	1347	110
m1.3-b1.5-g0	1419	103
m1.3-b1.6-g0	1495	95
MESO1 B		
m1.4-b1.2-g0	1271	118
m1.4-b1.3-g0	1346	110
m1.4-b1.4-g0	1420	103
m1.4-b1.5-g0	1496	95
m1.4-b1.6-g0	1572	88
MESO2 A		
m2-b1.2-g0	785.3	167
m2-b1.3-g0	858.8	159
m2-b1.4-g0	934.2	152
m2-b1.5-g0	1010	144
m2-b1.6-g0	1084	137
MESO2 B		
m3-b1.2-g0	1019	143
m3-b1.3-g0	1095	136
m3-b1.4-g0	1170	128
m3-b1.5-g0	1245	120
m3-b1.6-g0	1319	113
MESO2 C		
m4-b1.2-g0	635.5	182
m4-b1.3-g0	711.4	174
m4-b1.4-g0	784.9	167
m4-b1.5-g0	864.5	159
m4-b1.6-g0	935.8	152
REV1		
m1.5-b3.4-g0c	1990	46
m1.6-b3.4-g0c	2061	38
m1.7-b3.4-g0c	2135	31
m1.8-b3.4-g0c	2210	23

IV. Conclusion

A set of thermotropic ionic liquid crystal (TILC) molecules were simulated using Density Functional Theory (DFT), along with a set of non-ionic thermotropic liquid crystals, for the purpose of finding a TILC with correct properties to act as a dendrite-inhibiting electrolyte in next-generation lithium metal batteries (LMBs).

A strong correlation was found between the set from Mizumura *et al.* between zero point vibrational energy and the isotropic–smectic phase transition on cooling. These phase transition temperatures were then predicted for other molecules using the aforementioned correlation.

A State-of-the-Art analysis was made in the full thesis in regards to the use of computational chemistry in materials and molecule discovery. The importance of finding a synergetic workflow between theory and experiment, in particular where the former suggests the latter instead of being used as to post-rationalize experiment, was highlighted. The rise in prominence and potential of using data-driven techniques such as machine learning (ML) in computational chemistry was also highlighted.

The main principles of DFT were reviewed in the full thesis, going over various methods but focusing on Kohn-Sham DFT (KS-DFT). The five levels of functionals used to approximate the elusive exchange-correlation energy and their mathematics were reviewed. Advantages and disadvantages of DFT, as well as guiding principles for choosing DFT functionals, were discussed. It is recommended to use as high level functionals as computational resources allow, and to always use dispersion correction methods.

The possibilities of using ML methods to completely bypass the speed-limiting Kohn-Sham (KS) equation for more efficient linearly-scaling DFT was also reviewed in the full thesis. A combination of KS-DFT and ML-DFT is suggested, where KS-DFT is used to produce high-quality but computationally expensive data for ML-DFT to train on, which in turn will be able to produce data similar of quality in a fraction of time.

A computational workflow model for high-throughput DFT calculations was created and automated via code to facilitate closed-loop discovery. Calculations were successfully used to predict isotropic-smectic phase transition temperatures. Improvements to the source TILCs, such as elongating the alkyl chain of the promesogenic group and adding a methyl to the functional group in order to lower said temperature, were suggested, thus guiding future experiment. New experimental data is easy to integrate in the model and the amount of compounds calculated may be up-scaled significantly without significant additional work.

The use of multivariate regression and ML models is strongly advised to improve the model and its applicability to non-similar systems. With more data points, there is great potential in having a reliable method of predicting some macro-level properties (in this case phase transition temperatures) through DFT without needing to simulate multi-molecule systems.

Acknowledgment

This thesis is part of VTT's contribution to the HIDDEN[10] project, which has received funding from the European Union's Horizon 2020 research and innovation programme under grant agreement No 957202.

References

[1] J. Tollefson, "What the war in ukraine means for energy, climate and food," *Nature*, vol. 604, no. 7905, pp. 232–233, Apr. 2022.

[2] M. S. Whittingham, "History, evolution, and future status of energy storage," *Proceedings of the IEEE*, vol. 100, no. Special Centennial Issue, pp. 1518–1534, May 2012.

[3] G. Crabtree, "The coming electric vehicle transformation," *Science*, vol. 366, no. 6464, pp. 422–424, Oct. 2019.

[4] M. K. Aslam *et al.*, "How to avoid dendrite formation in metal batteries: Innovative strategies for dendrite suppression," *Nano Energy*, vol. 86, p. 106 142, Aug. 2021.

[5] P. Raynes, "LIQUID CRYSTALS — second edition, by s CHANDRASEKHAR, cambridge university press, (1992), ISBN 0-521-41747-3 (HB), ISBN 0-521-42741-x (PB)," *Liquid Crystals Today*, vol. 3, no. 3, pp. 7–7, Nov. 1993.

[6] "Liquid Crystals." Accessed online on 23.02.2023. (Jan. 2023), [Online]. Available: `https://chem.libretexts.org/Bookshelves/Physical_and_Theoretical_Chemistry_Textbook_Maps/Supplemental_Modules_(Physical_and_Theoretical_Chemistry)/Physical_Properties_of_Matter/States_of_Matter/Liquid_Crystals`.

[7] K. Goossens, K. Lava, C. W. Bielawski, and K. Binnemans, "Ionic liquid crystals: Versatile materials," *Chemical Reviews*, vol. 116, no. 8, pp. 4643–4807, Apr. 2016.

[8] K. Binnemans, "Ionic liquid crystals," *Chemical Reviews*, vol. 105, no. 11, pp. 4148–4204, Nov. 2005.

[9] K. V. Axenov and S. Laschat, "Thermotropic ionic liquid crystals," *Materials*, vol. 4, no. 1, pp. 206–259, Jan. 2011.

[10] "The hidden project." (2022), [Online]. Available: `https://hidden-project.eu/`.

[11] Y. Mizumura *et al.*, "Self-assembled liquid-crystalline ion conductors: Odd-even effects of flexible spacers binding a carbonate moiety and an aliphatic rod-like core on phase transition properties and ion conductivities," *Bulletin of the Chemical Society of Japan*, vol. 92, no. 7, pp. 1226–1233, Jul. 2019.

[12] R. J. Mandle *et al.*, "Engineering mesophase stability and structure via incorporation of cyclic terminal groups," *Journal of Materials Chemistry C*, vol. 10, no. 15, pp. 5934–5943, 2022.

[13] E. Makara, "Quantum chemical investigation of thermotropic ionic liquid crystals to predict phase transition temperatures," English, Master's thesis, Aalto University. School of Chemical Engineering, 2023, p. 81.

[14] LCI Systems. "Liqcryst." Accessed online on 16.02.2023. (), [Online]. Available: `https://www.lci-systems.com/liqcryst/`.

[15] "TURBOMOLE V7.2 2017, a development of University of Karlsruhe and Forschungszentrum Karlsruhe GmbH, 1989-2007, TURBOMOLE GmbH, since 2007." (), [Online]. Available: `https://www.turbomole.com`.

[16] R. Ahlrichs, M. Bar, M. Haser, H. Horn, and C. Kolmel, "Electronic structure calculations on workstation computers: The program system turbomole," *Chemical Physics Letters*, vol. 162, no. 3, pp. 165–169, Oct. 1989.

[17] O. Treutler and R. Ahlrichs, "Efficient molecular numerical integration schemes," *The Journal of Chemical Physics*, vol. 102, no. 1, pp. 346–354, Jan. 1995.

[18] M. V. Arnim and R. Ahlrichs, "Performance of parallel TURBOMOLE for density functional calculations," *Journal of Computational Chemistry*, vol. 19, no. 15, pp. 1746–1757, Nov. 1998.

[19] C. Adamo and V. Barone, "Toward reliable density functional methods without adjustable parameters: The PBE0 model," *The Journal of Chemical Physics*, vol. 110, no. 13, pp. 6158–6170, Apr. 1999.

[20] M. Ernzerhof and G. E. Scuseria, "Assessment of the perdew–burke–ernzerhof exchange-correlation functional," *The Journal of Chemical Physics*, vol. 110, no. 11, pp. 5029–5036, Mar. 1999.

[21] K. Eichkorn, O. Treutler, H. ohm, M. Haser, and R. Ahlrichs, "Auxiliary basis sets to approximate coulomb potentials," *Chemical Physics Letters*, vol. 240, no. 4, pp. 283–290, Jun. 1995.

[22] K Eichkorn, O Treutler, H ohm, M Haser, and R Ahlrichs, "Auxiliary basis sets to approximate coulomb potentials (chem. phys. letters 240 (1995) 283-290)," *Chemical Physics Letters*, vol. 242, no. 6, pp. 652–660, Sep. 1995.

[23] K. Eichkorn, F. Weigend, O. Treutler, and R. Ahlrichs, "Auxiliary basis sets for main row atoms and transition metals and their use to approximate coulomb potentials," *Theoretical Chemistry Accounts: Theory, Computation, and Modeling (Theoretica Chimica Acta)*, vol. 97, no. 1-4, pp. 119–124, Oct. 1997.

[24] M. Sierka, A. Hogekamp, and R. Ahlrichs, "Fast evaluation of the coulomb potential for electron densities using multipole accelerated resolution of identity approximation," *The Journal of Chemical Physics*, vol. 118, no. 20, pp. 9136–9148, May 2003.

[25] F. Weigend and R. Ahlrichs, "Balanced basis sets of split valence, triple zeta valence and quadruple zeta valence quality for h to rn: Design and assessment of accuracy," *Physical Chemistry Chemical Physics*, vol. 7, no. 18, p. 3297, 2005.

[26] F. Weigend, "Accurate coulomb-fitting basis sets for h to rn," *Physical Chemistry Chemical Physics*, vol. 8, no. 9, p. 1057, 2006.

[27] "Chirality and Stereoisomers." Accessed online 20.02.2023. (Jan. 2023), [Online]. Available: `https://chem.libretexts.org/Bookshelves/Organic_Chemistry/Supplemental_Modules_(Organic_Chemistry)/Chirality/Chirality_and_Stereoisomers`.

[28] "Stereoisomers: Ring Conformations." Accessed online on 20.02.2023. (Jan. 2023), [Online]. Available: `https://chem.libretexts.org/Bookshelves/Organic_Chemistry/Supplemental_Modules_(Organic_Chemistry)/Chirality/Stereoisomers/Stereoisomers\%3A_Ring_Conformations`.

[29] S. Saunders and H. R. Brown, Eds., *The Philosophy of Vacuum*, en. Oxford, England: Clarendon Press, Jun. 1991, ISBN: 9780198244493.

[30] P. W. Milonni, *The Quantum Vacuum*, en. San Diego, CA: Academic Press, Jan. 1994, ISBN: 978-0-08-057149-2.

[31] M. H. Samha, J. L. H. Wahlman, J. A. Read, J. Werth, E. N. Jacobsen, and M. S. Sigman, "Exploring structure–function relationships of aryl pyrrolidine-based hydrogen-bond donors in asymmetric catalysis using data-driven techniques," *ACS Catalysis*, vol. 12, no. 24, pp. 14 836–14 845, Nov. 2022.

[32] G. B. Goh, N. O. Hodas, and A. Vishnu, "Deep learning for computational chemistry," *Journal of Computational Chemistry*, vol. 38, no. 16, pp. 1291–1307, Mar. 2017.

[33] T. Melin, R. Lundström, and E. J. Berg, "Revisiting the ethylene carbonate–propylene carbonate mystery with operando characterization," *Advanced Materials Interfaces*, vol. 9, no. 8, p. 2 101 258, Oct. 2021.